Slamming and Whipping Analysis in Preliminary Structural Design

Bruce L. Hutchison, P.E., (FSNAME, The Glosten Associates, Inc.)
Justin M. Morgan, P.E., (MSNAME, The Glosten Associates, Inc.)

Low-order parameterized methods presented are suitable for estimation of whipping responses without involved analysis. Multi-variate regression of response over parameter space make possible estimates during early design of the whipping frequency, the peak whipping-ending moment, and the time lag of that peak whipping-bending moment following the peak of the slamming impulse.

KEY WORDS

Slamming; whipping; non-uniform beam; Timoshenko beam.

INTRODUCTION

An estimate of whipping response due to slamming can help quantify the non-stationary contribution to overall bending moment from response to impulsive loads. A need has been identified for a quick and simple means of estimation suitable for early design. This paper is focused primarily on the midship bending moment due to whipping.

Recent work has focused on development of comprehensive numerical prediction methods for evaluating nonlinear, hull-girder bending moments. Papers by Fonseca, Antunes, and Soares (2006), and by Luo, Wan, and Gu (2007), present numerical models validated by test results. Jensen and Mansour (2002 and 2003) propose closed-form expressions for long-term, wave-induced bending moments, including whipping.

For early design work, these methods are generally too complex or require input that may not be available. This paper presents the results from a similar numerical model, with the simplification of assumptions applied to define the input parameters. This simple model is run over a range of input parameters. The resulting multi-variant regression equations permit the estimation of modal frequency and midship bending moments due to whipping based on characteristic ship parameters.

This paper focuses on the hull-girder response as a function of an assumed slam impulse. Stavovy and Chuang (1976) propose a method for determining slamming pressures analytically. Ochi and Motter (1973) present a comprehensive method for predicting slamming loads. Kapesenberg, Veer, Hackett, and Levadou (2003) and Luo, Wan, Qiu, and Gu (2007) discuss the duration and shape of the slamming impulse for stern slamming. The results of this paper are applicable to both bow and stern slamming due to the fore and aft symmetry of the distribution functions. Jensen *et al.* (2008) present some simple expressions that they suggest are suitable for estimating the magnitude of slamming impulses associated with "*slamming on flared bows, forward bottom parts and possibly flat stern areas of ships.*"

THE MODEL

The modeling method is based on low-order parameterizations described in the next section. Solutions have been obtained for a one-dimensional, free-free, non-uniform, Timoshenko beam finite element model implemented in NEiNASTRAN v9.1 (NASTRAN).

As background, the equations of a Timoshenko beam (without structural damping) are:

$$\rho_b A \frac{\partial^2 z}{\partial t^2} = \frac{\partial}{\partial x}\left\{ A\kappa G\left(\frac{\partial z}{\partial x} - \theta\right)\right\} + w \tag{1a}$$

$$\rho_b I \frac{\partial^2 \theta}{\partial t^2} = \frac{\partial}{\partial x}\left\{ EI\frac{\partial \theta}{\partial x}\right\} + A\kappa G\left\{\frac{\partial z}{\partial x} - \theta\right\}, \tag{1b}$$

where:
z	deflection of the beam
θ	angular displacement
ρ_b	density of the beam material
A	cross section area
E	elastic modulus
G	shear modulus
I	section moment of inertia
κ	Timoshenko shear coefficient
w	is the applied force distribution.

In the general case that includes large deflections, the Timoshenko beam is unlike the more familiar Euler-Bernoulli beam in that the angular deflection is another variable and not approximated by the slope of the deflection. However, for small deflections within the context of linear theory such as that implemented in NASTRAN, the angular deflection is commonly approximated by the slope of the deflection.

κ, called the Timoshenko shear coefficient, depends on the geometry. Normally, $\kappa = 5/6$ for a rectangular section. The shear coefficient and its longitudinal distribution are important parameters affecting the accuracy of predicted natural frequencies of the hull girder bending modes. Jensen (1983 and 2001) provides a comparison of various methods for determining shear coefficients.

w is a distributed load (force per length).

The global equation (including damping) of this study is given as Equation 2 as follows:

$$([m]+[A^\infty])\ddot{\vec{\xi}}(t)+[b]\dot{\vec{\xi}}(t)+([k]+[C])\vec{\xi}(t)=\vec{F}(t)\,, \qquad (2)$$

where:
- m structural mass
- A^∞ infinite frequency added mass
- b damping
- k structural stiffness
- C hydrostatic stiffness
- $\vec{F}$ applied external force (slamming force),

and $\vec{\xi}=[\vec{z}\ \vec{\theta}]^T$ is a generalized response vector, where $\vec{z}$ is the vector of nodal vertical displacements, and $\vec{\theta}$ is the vector of nodal rotations (which, for small displacements, may be approximated by $\partial z / \partial x$).

All terms of Equation 2 are spatial functions of location along the ship's hull girder. The $\rightarrow$ notation above all the vector terms indicates this dependence; i.e., $\vec{\xi}(t)=\xi(x,t)$ and $\vec{F}(t)=F(x,t)$. The spatial dependence of the matrix terms is implicit; e.g., $[m]\equiv[m(x)]$, $[A^\infty]\equiv[A^\infty(x)]$, $[b]\equiv[b(x)]$, and etc.

The infinite frequency added mass for vertical motion $[A^\infty]$ is obtained using Lewis form conformal mapping methods (Jensen 2001). As one approaches the infinite frequency limit, $[B(\omega\to\infty)]=[0]\equiv[B^\infty]$, so there is no radiation damping term corresponding to the infinite frequency added mass. Thus, [b] represents only structural damping.

Solutions to Equation 2 are found using the linear transient response solver in NASTRAN. Direct numerical integration is used in order to assign structural damping. Each vessel is modeled as a massless beam, with mass concentrated at 25 nodes (stations 0 through 20, plus two half-stations at either end). The beam section properties taper linearly between nodes.

The resulting multi-variate regression equations for response make possible early estimates of the whipping frequency, the peak whipping bending moment, and the time lag of that peak whipping bending moment following the peak of the slamming impulse.

PARAMETERIZATION

The low order parameterizations of virtual mass, hydrostatic, and effective beam stiffness distributions are related to basic design characteristics such as: Length, displacement, pitch, radius of gyration, midship beam-to-draft ratio, waterplane area and inertia (or BM_L), midship stiffness (EI), and a distribution 'shape' parameter. The low-order characterization of the slamming impulse is characterized by the total impulse, the peak force, and the initial rise time for each peak.

In order to limit the complexity and make this method suitable for early design, it was imperative to limit the parameters necessary to represent the various distributed ship properties represented by the matrices in Equation 2. Many equation forms were considered, and the following one-parameter equation was selected:

$$y(x)=Y_{MID}\left[1-\left|2\{(x/L)-0.5\}\right|\right]^\gamma, \qquad (3)$$

where:
- y is the distributed property
- Y_{MID} is the midship value of the distributed property
- L is the length over which the property is distributed
- γ is the parameter of the distribution.

Subject to $0\le x\le L$, this describes a distribution that is symmetric about midship (x/L=0.5). In principle, the distribution parameter can assume any positive value, but practical and realistic distributions are obtained with γ≥1. At midship, $y(x=0.5L)\equiv Y_{MID}$. When γ=1, the distribution is triangular, and as $\gamma\to\infty$, the distribution becomes rectangular (as in a uniform, rectangular barge). Figure 1 shows the non-dimensional distribution function over a range of γ values.
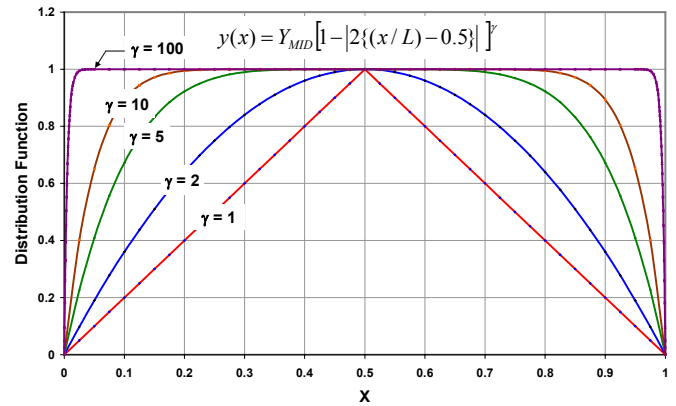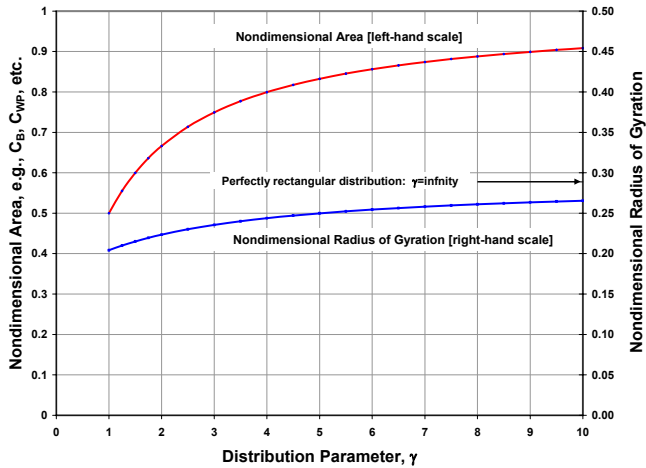

Figure 1. Example non-dimensional distribution functions.

The following integrals of Equation 3 give, respectively, the non-dimensional area and the non-dimensional radius of gyration:

$$\text{Area}=\int_0^L y(x)\,dx \qquad (4)$$

$$\text{Gyradius}=\sqrt{\frac{\int_0^L y(x)[x-0.5L]^2\,dx}{\int_0^L y(x)\,dx}}\,. \qquad (5)$$

These are shown in Figure 2, over the range 0<γ<10.

Figure 2. Example non-dimensional distribution functions.

The non-dimensional area corresponds to form coefficients such as C_B and C_{WP}. The non-dimensional gyradius relates to the mass moment of inertia of the hull or pitch added mass, and the longitudinal waterplane inertia. With only a single parameter for γ for each distribution, it is not possible to jointly match both an area and a gyradius. That would require higher-order parameterization. Also, because the chosen single parameter distribution is symmetric, it is not possible to match longitudinal first moment characteristics such as LCG or LCF. Despite these short-comings of the single parameter distribution, the ability to represent realistic ship distributions is acceptable for the purposes of early design.

Hull Geometric Distributions

As observed above, the one-parameter distribution adopted in the interest of simplicity leads to a fore-and-aft symmetry, as would be found in a true double-ended ship. This, of course, is an over-simplification for realistic commercial and naval vessels, but hopefully acceptable for assessments of whipping during early design. As a further simplification, it is presumed that the draft is constant over the entire length between forward and aft perpendiculars.

Remaining important hull geometry distributions are then the underwater sectional area and waterplane half-breadth. The underwater sectional area does not participate directly in Equation 2, but is necessary, along with the draft and waterline beam, to the estimation of hydrodynamic added mass using Lewis form conformal mapping.

Figure 3 presents, in non-dimensional form, a comparison of a one-parameter fit using Equation 3 to the actual sectional area distribution of the S-175 containership at 9.5 m draft. The ordinal values are all non-dimensionalized by the actual midship sectional area of the S-175. The distribution factor for sectional area, γ_1, is:

$$\gamma_1 = \left\{ \frac{1}{1 - C_B / C_{10}} \right\} - 1 \quad , \tag{6}$$

where C_{10} is the midship section area coefficient.
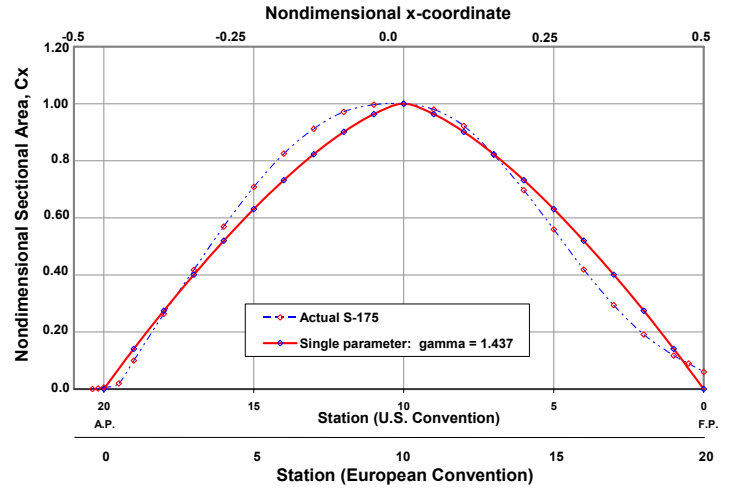
Figure 3. Comparison of single-parameter sectional area distribution for a S-175 container ship to actual at 9.5 m draft.

Figure 4 compares, in non-dimensional form, a one-parameter fit using Equation 3 to the actual waterplane half-breadth distribution of the S-175 containership at 9.5 m draft. The ordinal values are all non-dimensionalized by the actual midship half-breadth of the S-175. In the fit shown in Figure 4 for the half-breadth, both the fit midship half-breadth and the waterline length were also treated as parameters, which resulted in a small improvement in the quality of the fit. However, in the analysis that follows and in the early design whipping analysis method proposed in this paper, all distributions are presumed to extend over a common length, and midship ordinal values are presumably those available during early design. However, if actual distributions are available during early design it should be possible to obtain higher fidelity fits by adjusting the nominal length and/or midship ordinal values. The distribution factor for half-breadth, γ_2, used in the subsequent analyses is:

$$\gamma_2 = \left\{ \frac{1}{1 - C_{WP}} \right\} - 1 \quad . \tag{7}$$
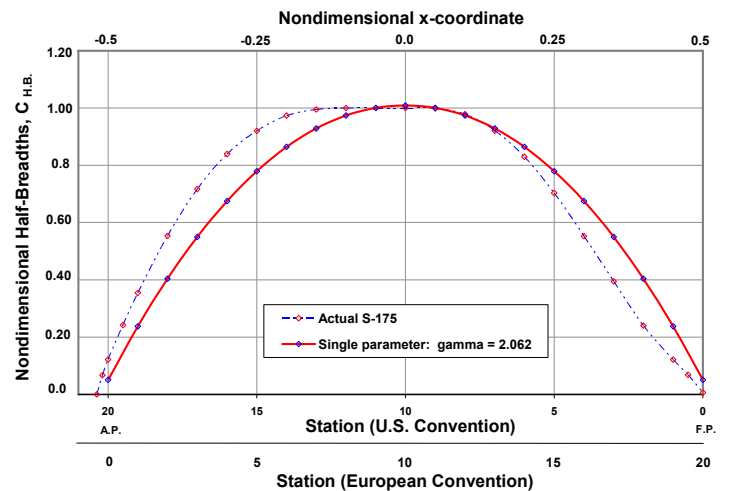
Figure 4. Comparison of single-parameter waterplane, half-breadth distribution for S-175 container ship to actual at 9.5 m draft.

The distribution of half-breadths not only figures in the estimation of hydrodynamic added mass, described further below, but also directly in the hydrostatic stiffness term [C] in Equation 2. The nodal hydrostatic stiffnesses in z are:

$$c_i = \rho \, g \, (2 \, b_i), \qquad (8)$$

where: c_i is the ith nodal hydrostatic stiffness

       b_i is the half-breadth of the ith node

       ρ fluid density

       g   is the acceleration of gravity.

Weight Distributions

Figure 5 compares two different one-parameter fits using Equation 3 with the standard weight distribution published in SEAWAY documentation (Journée 2001) for the S-175 containership at 9.5 m draft. The ordinal values are non-dimensionalized by $\rho g A_{10}$, where A_{10} is the midship underwater sectional area. Also, superimposed on the figure for reference, is the published weight distribution for the flexible S-175 model described in Wu and Hermundstad (2002).
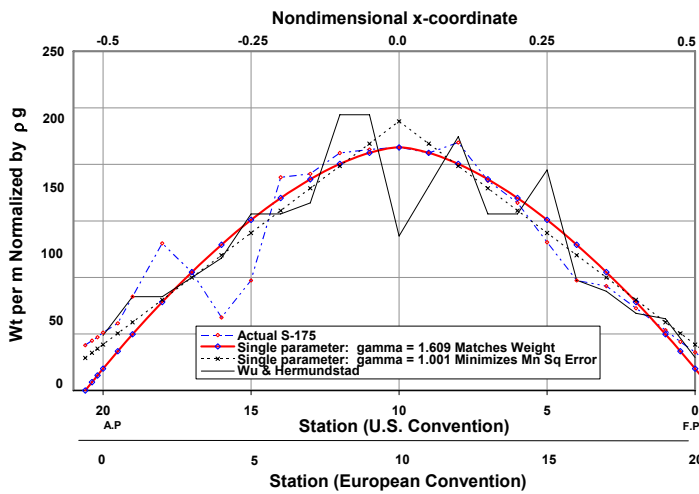
Figure 5. Comparison of single-parameter weight distribution for a S-175 container ship to actual at 9.5 m draft.

A single-parameter distribution with $\gamma_3 = 1.609$ and L/LBP=1.08 matches the weight of the S-175. A single parameter distribution with $\gamma_3 = 1.001$ (nearly triangular) and L/LBP=1.229 minimizes the mean squared error between the fit and the actual S-175 weight distribution.

The single parameter distribution matching weight appears to be a reasonable approximation for early design. Note that the current single parameter weight distribution formulation cannot model a load distribution with heavy ends.

The section-wise rotational inertia for the Timoshenko beam is approximated as a function of segment length and depth, as follows:

$$I_{yy} = m_{seg} \, C_k^2 \, (L_{seg}^2 + H^2). \qquad (9)$$

A value of 0.397 is assumed for the constant C_k, based on guidance (Vossers 1962) for thin-walled, rectangular sections. This value approximates the average section-wise rotational

inertia calculated from a 3D finite element model for a fine hull form.

Hydrodynamic Added Mass

Infinite frequency, heave added mass is estimated using Lewis form sections (Lewis 1929, and Jensen 2001). Lewis form conformal mapping requires, as input, only the local beam-to-draft ratio, B_x / H_x, of the 2-D section, and the local sectional area coefficient, $C_x = A_x /(B_x H_x)$. Figure 6 presents the distribution of non-dimensional added mass, $C_M = A^\infty /(\rho A_x)$, estimated using the Lewis form method for the S-175 containership.
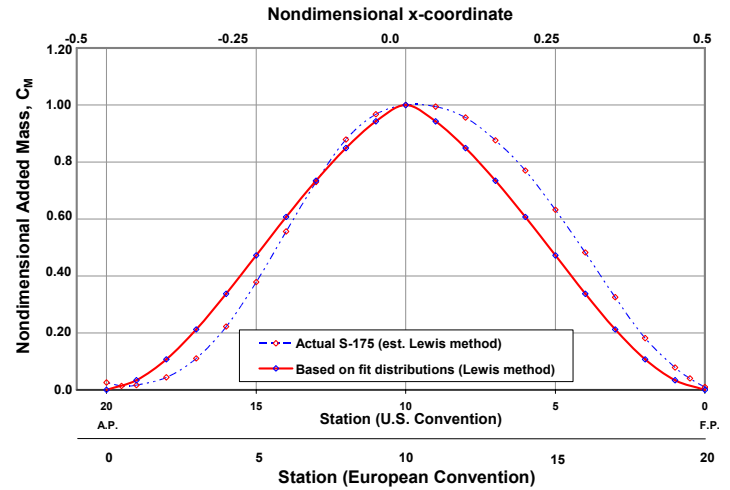
Figure 6. Comparison of heave added mass estimated by the Lewis method based on actual and fit distributions of beam, draft, and section area for a S-175 container ship at 9.5 m draft.

Figure 6 provides a comparison of the heave added mass calculated for both actual and fit distributions of beam, draft, and section area for the S-175 container ship at 9.5 m draft.

Structural Properties

Structural Damping: There is no radiation damping term corresponding to the infinite frequency added mass. Thus, only structural damping is assumed to be effective at whipping frequencies. Structural damping is modeled in NASTRAN as equivalent viscous damping, such that the input structural damping value only holds at one frequency and varies linearly at other frequencies. To simplify the model a constant value of 2%, critical damping was selected and applied at 2 Hz.

Beam Bending Stiffness, EI: Sectional inertia of the hull girder midship section is input as the ratio of the actual inertia to the ABS-required inertia (ABS Steel Vessel Rules 3-2-1/3.7). A range of values from 1 to 4 was selected for this variable, assuming that the ABS hull bending strength standard sets the minimum allowable inertia.

The distribution of sectional inertia is determined in accordance with Equation 3, the midship section inertia, and a fourth distribution variable for sectional inertia, γ_4. Figure 7 compares the one-parameter fit for sectional inertia using Equation 3, with a published (Wu and Hermundstad 2002) sectional inertia distribution for the S-175 containership.
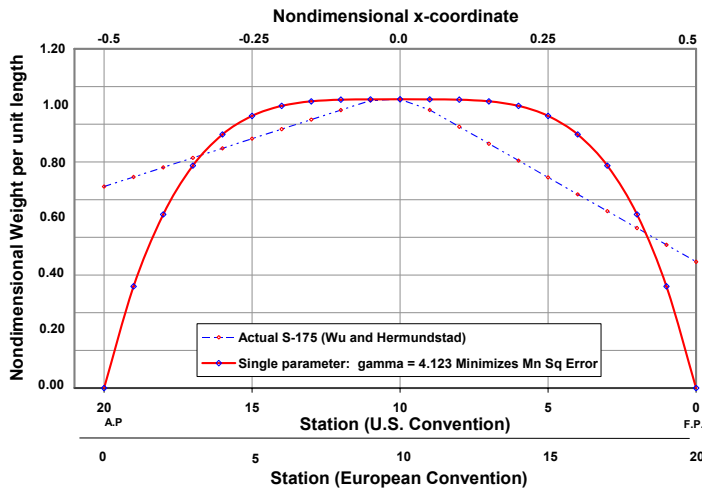
Figure 7. Comparison of single-parameter sectional inertia distribution for S-175 container ship to actual data.

Beam shear stiffness, AκG: The section-wise shear stiffness for the beam is given by:

$$A\kappa G ,\tag{10}$$

where: A   is the structural section area
κ   is the shear factor
G   is the shear modulus.

For simplicity, the shear factor is calculated from the assumed midship section, described above using Jensen's projected area method (Jensen 2001). Further development of this parameter in the model is warranted, given the strong influence of shear area on the resulting modal frequencies and given the known shortcomings of the chosen approach.

Structural section area of the midship section is estimated using a crude approximation of a typical cross section. The typical cross section is assumed to consist of shell, inner bottom, and inner side plating elements. A nominal shell plate thickness equal to 1.35 times ABS minimum thickness (ABS Steel Vessel Rules 3-2-2/3.17.2) is assumed to account for effective un-modeled stiffeners. Figure 8 illustrates the typical cross-section model. The distribution for sectional inertia is used to represent the structural section area distribution.
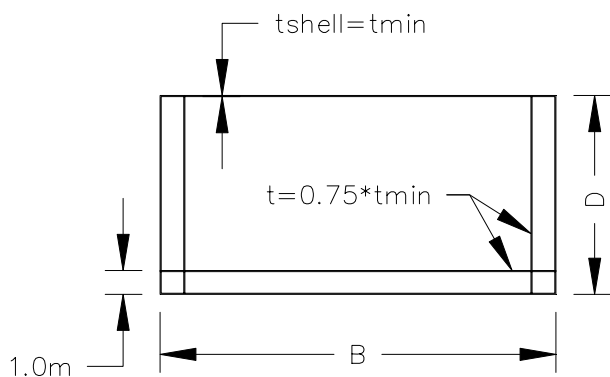
Figure 8. Typical cross-section model for calculating the midship structural section area.

Slam Impulse: The slam impulse, defined as $\int F \, dt$, is assumed to be held constant and applied at station 3. The impulse duration, T_d, and triangular shape presented by Ochi and Motter (1973), are used. Figure 9 illustrates the impulse:

$$T_d = 0.02487\sqrt{\frac{L}{g}} \qquad \text{[seconds]},\tag{11}$$

where L is the ship length.
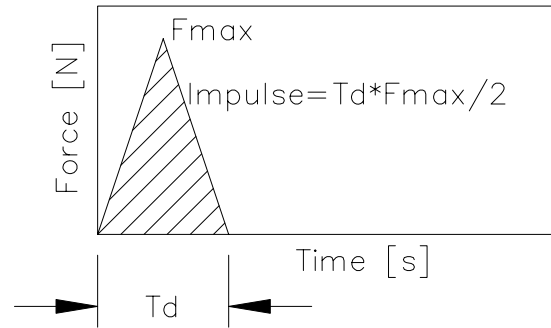
Figure 9. Slam impulse definition.

Since the modeled dynamic system is linear, if T_d is held constant, the impulse is linear with F_{max} and the midship bending moment scales linearly with F_{max}. The value of F_{max} assumed throughout this study is 10,000 kN, and the impulse is constant at 500 kN-s.

Methods to determine slam force, F(t), from hull geometry and vessel motions are not included in the scope of this paper. Jensen *et al.* (2008) provide simple equations from which the rise time and magnitude of slam impulse may be estimated. They suggest that their methods are suitable for bottom, bow flare, and possible stern slamming.

The methods here presented are not explicitly restricted to bottom slamming; but, by virtue of the longitudinal point of application of our slam impulse (i.e., 15% aft of F.P. or 15% forward of A.P.) and the modeled duration and shape, the regression equations presented later in this paper are probably most appropriate to bottom slamming, which possibly includes stern bottom slamming. However, for bow blare slam forces applied near the same location (i.e., 15% aft of F.P.), the regression equations given in this paper may provide a first approximation provided that the magnitude of the applied impulse is appropriate to a bow flare slam. As the model is linear bow bottom slamming followed by a bow flare slam, it could be modeled using linear superposition, though the development of this approach is left to future research.

RESULTS

A total of 6,561 distinct whipping cases were run using the foregoing described NASTRAN model. These 6,561 cases were generated with the parameter variations documented in Table 1.

Table 1. Parameter variations for 6,561 cases.

Parameter	From	To	Step
L/B	5	9	2
B/T	2	4	1
C_B	0.6	0.8	0.1
C_{WP}	0.6	0.9	0.15
γ_3 for weight	1	5	2
γ_4 for structural inertia	1	5	2
κ shear coefficient	0.25	0.5	0.125
I/I_{ABS}	1	4	1.5

Several variables were held constant in defining the matrix of cases: B/D = 1.75, C_{10} = 0.95, and L = 175 m.

The peak midship bending moment, the time, Δt, at which the peak midship bending moment occurs, the two-node[1] 'free-free' modal frequency, f_2, and the average zero-crossing period, $\overline{T}_Z$, of the first cycles in the first six seconds, were all captured as dependent data.

The following eight non-dimensional values were treated as independent variables.

Table 2. Non-dimensional independent variables.

x_1	B/L	Beam-to-length ratio
x_2	T/L	Draft-to-length ratio
x_3	C_B	Block coefficient
x_4	C_{WP}	Waterplane coefficient
x_5	γ_4	Distribution factor for structural inertia
x_6	$\dfrac{I}{[\,0.01\,L^4\,]}$	Midship structural inertia non-dimensionalized by $0.01\,L^4$
x_7	$\dfrac{A_{SHEAR}}{[\,0.01\,L^2\,]}$	Midship structural cross-section shear area non-dimensionalized by $0.01\,L^2$
x_8	$\dfrac{k_{yy}}{L}$	Pitch mass radius of gyration non-dimensionalized by L

The four non-dimensional dependent variables are as described in Table 3.

Table 3. Non-dimensional dependent variables.

y_1	$\dfrac{Max.\,B.M.}{(Impulse)\sqrt{gL}}$	Non-dimensional peak whipping bending moment amidship per unit impulse.
y_2	$\dfrac{\Delta t}{\sqrt{L/g}}$	Non-dimensional time at which the peak whipping bending moment amidship occurs relative to the start of the impulse.
y_3	$\dfrac{f_2}{\sqrt{g/L}}$	Non-dimensional two-node 'free-free' modal frequency.
y_4	$\dfrac{\overline{T}_Z}{\sqrt{L/g}}$	Non-dimensional average zero-crossing period of whipping response.

Using least-squared error regression methods, the dependent responses are fit to empirical quadratic multivariate models of the following form:

$$y_k = a_k + \sum_{i=1}^{8} b_{i,k}\,x_i + \sum_{i=1}^{8}\sum_{j=i}^{8} c_{ij,k}\,x_i x_j \,, \qquad (12)$$

where: a_k are the empirical (least squares) constant terms associated with the kth response

$b_{i,k}$ are the empirical (least squares) linear coefficients for the kth response

$c_{ij,k}$ are the empirical (least squares) quadratic coefficients for the kth response.

Tables of these least squares coefficients are provided in Appendix A.
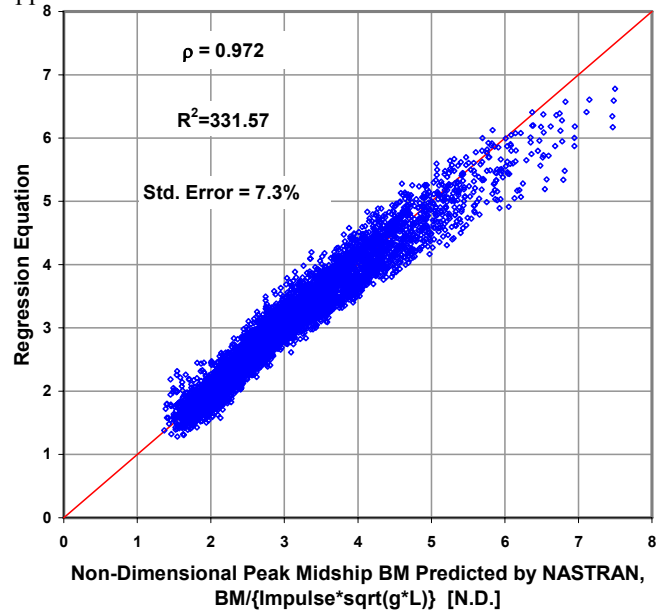
Figure 10. Correlogram between regression Equation 12 and peak midship whipping bending moment directly computed by NASTRAN.

Figure 10 presents a correlogram between actual peak non-dimensional midship bending moment, per unit impulse as computed by NASTRAN, and the corresponding regression equation. A correlation coefficient of $\rho = 0.972$ is achieved,

with a standard error of 7.3%; this is thought to be quite acceptable for early design.

The regression equation for non-dimensional bending moment, whose coefficients are given in Appendix A and whose correlation is illustrated in Figure 10, are all for the constant standard slam force distribution, with T_d =0.10 s, F_{max} =10,000 kN, and a resulting impulse of 500 kN-s. As previously observed, provided that the slam duration is held constant, the peak midship whipping bending moment will scale linearly with either F_{max} or impulse.

Figure 11 shows the correlogram for the time to maximum whipping bending moment. The correlation is not as good as that for bending moment or modal frequency, being only ρ=0.858, and the standard error is 13.9%. However, it should be observed that the distribution range is quite small when compared to wave and/or pitch periods.
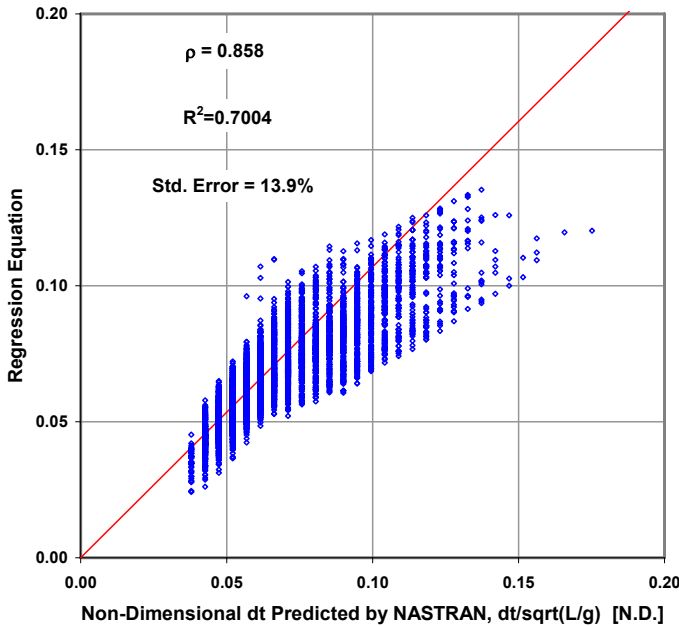
Figure 11. Correlogram between regression Equation 12 and time of occurrence of peak midship whipping bending moment computed by NASTRAN.

Figure 12 shows the correlogram between the regression equation for the two-node 'free-free' modal frequency and the corresponding values computed by NASTRAN. This regression 'fit' results in a correlation coefficient of ρ=0.975, and the standard error is 7.4%.
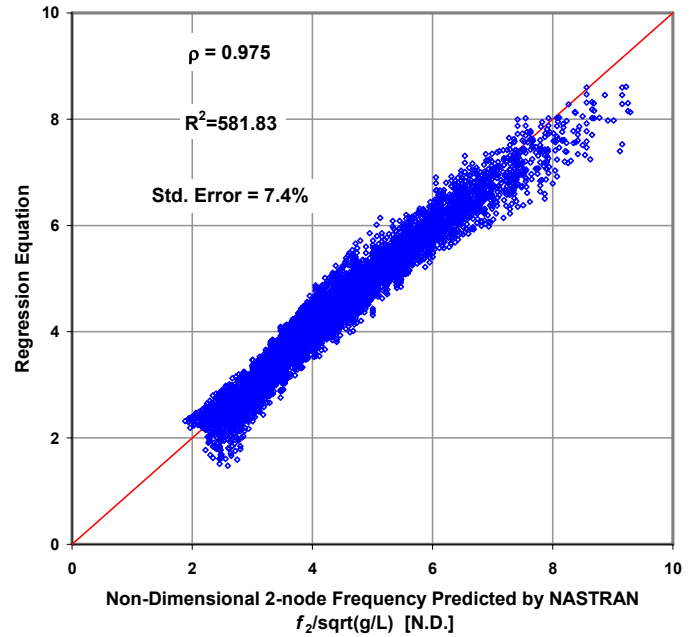
Figure 12. Correlogram between regression Equation 12 and the two-node 'free-free' modal frequency computed by NASTRAN.

Figure 13 shows the correlogram for the average zero-crossing period. The correlation coefficient is ρ=0.961, and the standard error is 7.7%.
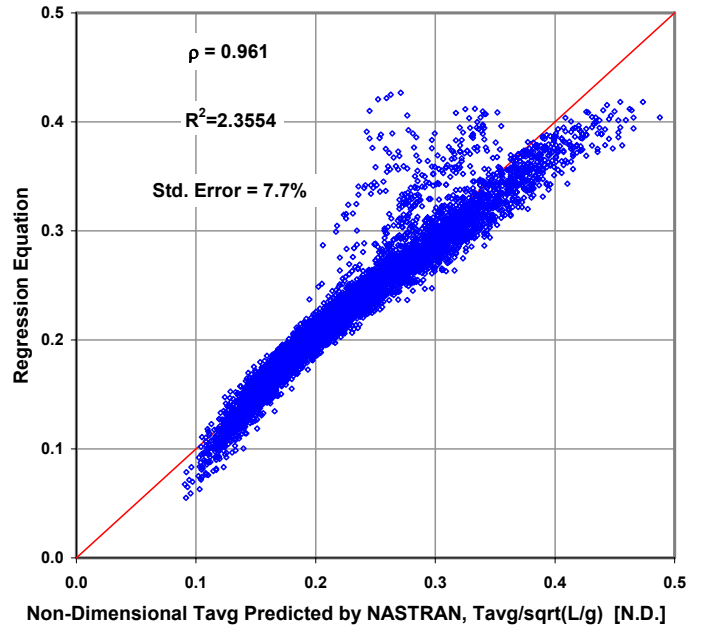
Figure 13. Correlogram between regression Equation 12 and average zero-crossing period computed by NASTRAN.

VALIDATION

This section compares the results of the presented single parameter distribution method with directly computed NASTRAN results for actual distributions, and with published numerical or experimental results. Further, it compares the presented regression results with direct NASTRAN calculations.

Comparison of NASTRAN to Published Results

One might expect a robust set of validation data, given the large body of work on the subject of whipping response. However, in practice, most papers fall short of the full documentation necessary to validate this work. Definitive data on the International Towing Tank Conference (ITTC) standard S-175 containership, arguably the most extensively studied vessel, is particularly elusive in the literature. The variation in first natural frequencies of the S-175 hull reported in Wu and Hermundstad (2002), Ramos, Incecik, and Soares (2000), and Gu, Shen, and Moan (2003), of 1.33, 1.17, and 1.60, respectively, reflects variation in assumed vessel parameters.

Weight distribution, structural stiffness, and shear area are the most commonly omitted vessel parameters. On the loading side, the slamming impulse is not always documented, and the associated slam-induced whipping moment is not isolated from the total bending moment.

Examples of the application of the presented method are provided for a naval frigate studied in both McTaggart *et al.* (1997) and Fonseca, Antunes, and Soares (2006). Table 4 compares the natural frequencies for the first three bending modes. The third and fourth columns compare respectively, the

- estimated natural frequencies predicted by NASTRAN using the distributions generated from single parameter fits, and
- corresponding estimates using "actual" weight, inertia, and area distributions.

Table 4. Natural frequencies for the first three vertical bending modes for the McTaggart frigate.

Natural Frequency [Hz]				
Mode	McTaggart (1997)	Fonseca (2006)	NASTRAN Single Parameter Distributions	NASTRAN Actual Distributions
2	1.42	1.30	1.51	1.30
3	2.69	3.00	2.86	2.52
4	4.48	5.49	4.16	3.87

The whipping vertical bending moment, calculated by Fonseca, Antunes, and Soares (2006) for the McTaggart frigate, is approximately 94 Nm per unit slam impulse centered about station 4. The present NASTRAN model predicts a value of 124 Nm per unit slam impulse centered at station 3 and the regression equations predict a value of 92 Nm per unit slam impulse.

Examples of the application of the presented method are also provided for the S-175 containership studied in *Wu and Hermundstad (2002)*, *Ramos et al.* (2000), and *Gu et al.* (2003). Comparisons of the first three bending modal frequencies are provided in Table 5. Note that the shear stiffness and shear distribution of the S-175 model are not published in these references. The degrading correlation of the natural frequencies for the presented method to experimental data at higher modes is attributed to the missing shear distribution information, and the poor approximation of inertia outside midships provided by the one parameter inertia distribution fit shown in Figure 7 (presented on page 5).

Table 5. Natural frequencies for the first three vertical bending modes for the S-175 containership.

Natural Frequency [Hz]				
Mode	Wu and Hermundstad (2002)	Ramos (2000)	Gu (2003)	NASTRAN Single Parameter Distributions
2	1.33	1.17	1.60	1.35
3	3.24	3.16		2.52
4	6.16	6.44		3.67

Comparison of Regression Predictions

Table 6 provides results of the regression equations and the NASTRAN models for the S-175 and McTaggart frigate. The errors found between regression and directly calculated NASTRAN results are larger than one might expect based on the standard deviation of the fit. However, two regression parameters fall outside the data range for each vessel. Both the frigate and containership are fine form vessels with block coefficients less than 0.6, the minimum value included in the evaluation set. In the case of the containership the weight distribution factor exceeds the range of parametric variation. The frigate's shear area is lower than the minimum value in the assumed parameter range.

Table 6. Comparison of regression results and direct calculation.

Parameter	Units	Regression	NASTRAN (direct calculation)	Error
S-175				
Max B.M.	N-m / unit impulse	125.79	150.15	-16.2%
Δt	s	0.24	0.24	0.2%
f_2	Hz	1.20	1.35	-10.8%
$\overline{T}_z$	s	0.84	0.75	11.8%
Frigate				
Max B.M.	N-m / unit impulse	92.37	123.86	-25.4%
Δt	s	0.29	0.22	31.9%
f_2	Hz	1.23	1.51	-18.4%
$\overline{T}_z$	s	0.88	0.67	30.9%

Better agreement between the NASTRAN and regression results comes from arbitrarily setting the outlying parameters to values within the evaluation range. The errors in bending moment calculated for these modified models were 0.6 and 1.6 times standard deviation for the frigate and S-175, respectively. By comparison, Table 6 shows values of 2.2 and 3.5 times standard deviation.

CONCLUSIONS

Eight independent variables describing non-uniform beam ship whipping cases were varied over three values each. Infinite frequency hydrodynamic added mass distributions for each case were generated using Lewis sections. NEiNASTRAN was used to predict the whipping response of each of the resulting six-thousand five-hundred and sixty-one (6561) different whipping cases. Multiple linear regression models were fit to the resulting data set, resulting in excellent fits for the peak midship bending moment, two-node 'free-free' wet natural frequency, and average whipping period. Though the regression fit for the time from slam onset to the peak midship bending moment was not quite as good, the distribution range is quite small when compared to wave and/or pitch periods.

The NASTRAN solutions were validated against published results for a frigate and for the S-175 containership. The regression equations are suitable for early design and were demonstrated though application to the frigate and the S-175 containership.

RECOMMENDATIONS FOR FURTHER WORK

Recommendations for further research include adopting asymmetric distributions with the capability to account for fore/aft asymmetry and, also, distributions capable of modeling hogging mass distributions.

The range of parametric variation should be expanded to evaluate a larger set of vessels. As a minimum, the data set should encompass the vessels with data available for validation.

This current work has confirmed the findings of previous researchers that the shear stiffness is an important model parameter. Future research should include improved models for shear stiffness, and the further examination of the sensitivity of whipping response to variations amongst shear stiffness models.

Goals for future research include variations of impulse location, duration, and rise slope in order to better represent bow flare slamming. Future studies should also examine the separation and time-domain linear superposition of whipping responses due to bow bottom slamming followed by bow flare slamming.

ACKNOWLEDGEMENTS

REFERENCES

FONSECA, N., ANTUNES, E. and SOARES, C., (2006). "Whipping Response of Vessels with Large Amplitude Motions," *Proceedings of OMAE 2006*.

GU X., SHEN, J., and MOAN, T., (2003). "Efficient and Simplified Time Domain Simulation of Nonlinear Responses of Ships in Waves," *Journal of Ship Research*, Vol. 47, No. 3, September 2003, pp 262-273, SNAME.

JENSEN, J.J., (2001). "Load and Global Response of Ships," *Elsevier Ocean Engineering Book Series*, Vol. 4.

JENSEN, J.J., (1983). "On the Shear Coefficient in Timoshenko's Beam Theory," *Journal of Sound and Vibration*, Vol. 87(4), pp 621-635.

JENSEN, J.J., and MANSOUR, A.E., (2002). "Estimation of Ship Long-Term Wave-Induced Bending Moment Using Closed-Form Expressions," *RINA Transactions*.

JENSEN, J.J., and Mansour, A.E., (2003). "Estimation of the Effect of Green Water and Bow Flare Slamming on the Wave-Induced Vertical Bending Moment Using Closed-Form Expressions," *Proceedings of the 3rd International Conference on Hydroelasticity in Marine Technology*, The Oxford University Press, Oxford, pp 155-161, September 2003.

JENSEN, J.J., and PEDERSEN, P.T., (1978). "Wave-Induced Bending Moments in Ships – A Quadratic Theory," *Transactions*, RINA, pp 151-165.

JENSEN, J.J., PEDERSEN, P.T., SHI, B., WANG, S., PETRICIC, M., and MANSOUR, A.E., (2008). "Wave Induced Extreme Hull Girder Loads on Containerships," SNAME 2008 SMTC&E, to be published in 2008 *Transactions*.

JOURNÉE, J.M.J., (2001). "User Manual of SEAWAY," Release 4.19, Delft University of Technology, Report 1212a.

KAPSENBERG, G.K., van't VEER, A.P., HACKETT, J.P., and VASILAKOS, J., (2003). "The Impact of Evolutionary Acquisition on Naval Ship Design," *Transactions*, SNAME.

LEWIS, F.M., (1929). "The Inertia of Water Surrounding a Vibrating Ship," *Transactions*, SNAME.

LUO, H., WAN, Z. QIU, Q., and GU, X., (2007). "Numerical Simulation of Whipping Responses induced by Stern Slamming Loads in Following Waves," Ninth International Conference on Fast Sea Transportation, FAST.

MCTAGGART, K., DATTA, I., STIRLING, A., GIBSON, S., AND GLEN, I., (1997). "Motions and Loads of a Hydroelastic Frigate Model in Severe Seas," *Transactions*, SNAME.

OCHI, M., and MOTTER, L., (1973). "Prediction of Slamming Characteristics and Hull Responses for Ship Design," *Transactions*, SNAME.

PEDERSEN, T., (2000). "Wave Load Prediction – a Design Tool," Ph.D. thesis, Department of Naval Architecture and Offshore Engineering, Technical University of Denmark.

RAMOS J., INCECIK A., and GUEDES SOARES, C., (2000). "Experimental Study of Slam-Induced Stresses in a Containership," *Marine Structures*, Vol. 13, pp 25-51.

STAVOVY, A., and CHUANG, S., (1976). "Analytical Determination of Slamming Pressures for High-Speed Vehicles in Waves," *Journal of Ship Research*, Vol. 20, No. 4, December 1976, SNAME.

VOSSERS, G., (1962). "Fundamentals of the Behaviour of Ships in Waves," *International Shipbuilding Progress,* Vol. 9, No. 93, May 1962.

WU, M., and HERMUNDSTAD, O.A., (2002). "Time-domain simulation of wave-induced nonlinear motions and loads and its applications in ship design," *Marine Structures*, Vol. 15, pp 561-597.

APPENDIX A – Regressed Coefficients for Equation 12

		B.M. [N.D.]		Δt [N.D.]		f₂ [N.D.]		Tavg [N.D.]	
R^2:			331.57		0.698		581.83		2.36
ρ:			0.972		0.858		0.975		0.961
Std. Error:			7.3%		13.9%		7.4%		7.7%
		k=1		k=2		k=3		k=4	
Constant:		$a_k =$	1.471E+01	$a_k =$	6.847E-02	$a_k =$	6.433E+00	$a_k =$	-2.088E-01
i	j	ρ	$b_{i,k}, c_{ij,k}$	ρ	$b_{i,k}, c_{ij,k}$	ρ	$b_{i,k}, c_{ij,k}$	ρ	$b_{i,k}, c_{ij,k}$
1		0.2754	-5.462E+01	-0.3414	2.072E-01	0.3991	-2.957E+01	-0.3923	1.164E+00
2		0.3702	-7.710E+01	-0.3899	2.308E-01	0.5003	-1.102E+02	-0.4664	2.292E+00
3		0.0705	1.129E+01	0.0005	-7.537E-02	-0.0512	-5.029E+00	-0.0181	-5.177E-02
4		0.5386	-5.922E+00	-0.2048	-3.737E-02	0.2307	5.692E+00	-0.2834	1.201E-01
5		0.0656	5.039E-01	-0.0051	-2.477E-02	0.4353	2.111E+00	-0.1755	-4.111E-02
6		0.3266	3.435E-01	-0.4099	-7.965E-04	0.2746	1.536E-01	-0.4528	-1.072E-02
7		-0.1220	8.331E+00	0.0823	-6.450E-02	-0.2176	1.404E+00	0.1733	9.059E-02
8		0.3594	-6.563E+01	-0.0529	3.180E-01	0.1094	1.337E+01	-0.1441	1.898E+00
1	1	-0.2720	5.502E+01	0.3400	-2.518E-01	-0.3946	5.753E+01	0.3900	-2.567E+00
1	2	-0.3527	1.099E+02	0.4029	1.479E+00	-0.4882	1.831E+02	0.4722	1.696E+00
1	3	-0.2172	1.284E+01	0.3070	-2.563E-01	-0.3792	3.082E+01	0.3437	-9.184E-01
1	4	0.5167	-3.498E-01	-0.3988	4.563E-01	0.4519	-1.928E+01	-0.4794	1.326E+00
1	5	0.0540	-5.436E-02	-0.1425	9.543E-04	-0.2173	-3.807E+00	-0.0015	1.987E-02
1	6	-0.1554	-3.650E-01	0.2160	-7.324E-03	-0.0773	-4.141E-02	0.2338	-1.563E-02
1	7	-0.1928	3.814E-01	0.1898	-3.743E-01	-0.3059	1.149E+00	0.2727	4.947E-01
1	8	-0.3630	8.506E+01	0.3322	4.845E-01	-0.4027	-3.238E+01	0.4079	7.237E-01
2	2	-0.3443	1.208E+02	0.3775	-9.983E-01	-0.4664	2.252E+02	0.4472	-5.261E+00
2	3	0.3364	-3.228E+01	-0.3736	4.778E-01	0.4922	-1.813E+01	-0.4409	2.009E+00
2	4	-0.5236	6.991E+01	0.4353	-1.885E-01	-0.5322	5.760E+01	0.5264	-2.362E+00
2	5	0.1583	-5.654E-01	-0.2307	3.526E-02	-0.0520	-5.385E-01	-0.1217	9.681E-03
2	6	-0.0386	-3.653E-01	0.1165	-6.407E-03	0.0570	-6.405E-01	0.1121	-2.013E-02
2	7	0.2787	-7.750E+00	-0.2664	-3.240E-01	0.4059	-1.168E+01	-0.3639	-4.600E-01
2	8	-0.4281	3.570E+01	0.3866	-7.415E-01	-0.5043	3.748E+01	0.4800	3.981E-01
3	3	0.0706	9.722E-01	-0.0001	-8.601E-02	-0.0510	2.760E+00	-0.0187	-2.552E-01
3	4	0.4065	-9.763E+00	-0.1744	1.887E-01	0.2189	-3.845E+00	-0.2253	4.467E-01
3	5	0.0795	4.177E-02	-0.0034	3.673E-03	0.4169	1.681E-01	-0.1730	8.267E-03
3	6	-0.3241	-3.061E-03	0.3850	4.694E-04	-0.2452	-1.134E-01	0.4315	5.633E-04
3	7	-0.0942	9.718E-01	0.0793	1.857E-02	-0.2218	-2.264E+00	0.1585	-3.013E-02
3	8	0.1486	-2.425E+01	-0.0314	2.417E-01	0.1035	2.206E+00	-0.0674	4.822E-01
4	4	0.5406	-4.345E+00	-0.2037	-2.237E-02	0.2327	-5.130E+00	-0.2844	1.688E-01
4	5	0.0973	-1.991E-01	-0.0626	6.040E-03	-0.3303	-7.050E-01	0.0818	8.467E-03
4	6	-0.1484	-1.134E-01	0.3371	-1.285E-03	-0.2027	4.257E-02	0.3505	1.015E-04
4	7	0.3222	-2.520E+00	-0.1569	-5.441E-02	0.2850	1.469E+00	-0.2666	-2.221E-01
4	8	-0.6294	6.131E+01	0.2042	-3.062E-01	-0.2529	1.299E+01	0.3112	-2.442E+00
5	5	-0.0585	-1.587E-02	0.0090	-2.281E-04	-0.3951	-1.229E-01	0.1585	2.652E-03
5	6	0.2693	2.319E-03	-0.3034	-1.708E-04	0.5264	2.290E-02	-0.4287	-2.329E-04
5	7	0.0187	-8.488E-02	-0.0636	1.028E-02	-0.2228	3.401E-01	0.0419	4.916E-03
5	8	-0.0099	-9.619E-01	-0.0117	7.214E-02	-0.4098	-1.829E+00	0.1514	1.872E-02
6	6	-0.2494	-1.213E-03	0.3161	8.191E-05	-0.1805	-3.512E-03	0.3545	2.573E-04
6	7	0.1744	5.928E-02	-0.2624	4.366E-04	0.0921	3.106E-02	-0.2525	3.415E-05
6	8	-0.2664	-4.030E-01	0.3972	-4.113E-03	-0.2565	3.061E-01	0.4244	-5.006E-04
7	7	0.1241	-3.820E+00	-0.0827	1.292E-01	0.2163	-3.422E+00	-0.1707	-4.623E-02
7	8	0.1926	-1.809E+01	-0.0902	4.560E-02	0.2320	4.820E+00	-0.1970	-2.242E-01
8	8	-0.3591	3.954E+01	0.0528	-9.345E-01	-0.1097	-6.097E+01	0.1442	-2.237E-01

APPENDIX B – S-175 Containership Example

The following example is for the 175 m S-175 containership.

				B.M. [N.D.]	Δt [N.D.]	f_2 [N.D.]	Tavg [N.D.]
		Constant:		1.471E+01	6.847E-02	6.433E+00	-2.088E-01
x_i	x_j	i	j	k=1	k=2	k=3	k=4

		x_i	x_j	i	j	k=1	k=2	k=3	k=4
x1	B/L	0.145		1		-7.928E+00	3.008E-02	-4.292E+00	1.689E-01
x2	T/L	0.054		2		-4.185E+00	1.253E-02	-5.984E+00	1.244E-01
x3	C_B	0.572		3		6.460E+00	-4.311E-02	-2.877E+00	-2.962E-02
x4	C_{WP}	0.696		4		-4.122E+00	-2.601E-02	3.962E+00	8.360E-02
x5	γ_4	6.214		5		3.131E+00	-1.539E-01	1.312E+01	-2.555E-01
x6	$I/[0.01\ L]^4$	15.324		6		5.264E+00	-1.220E-02	2.353E+00	-1.642E-01
x7	$A_{SHEAR}/[0.01\ L]^2$	0.166		7		1.381E+00	-1.069E-02	2.326E-01	1.501E-02
x8	k_{yy}/L	0.240		8		-1.575E+01	7.631E-02	3.210E+00	4.555E-01
		0.145	0.145	1	1	1.159E+00	-5.304E-03	1.212E+00	-5.407E-02
		0.145	0.054	1	2	8.656E-01	1.166E-02	1.443E+00	1.336E-02
		0.145	0.572	1	3	1.066E+00	-2.128E-02	2.559E+00	-7.625E-02
		0.145	0.696	1	4	-3.533E-02	4.610E-02	-1.948E+00	1.339E-01
		0.145	6.214	1	5	-4.903E-02	8.607E-04	-3.434E+00	1.792E-02
		0.145	15.324	1	6	-8.118E-01	-1.629E-02	-9.211E-02	-3.477E-02
		0.145	0.166	1	7	9.174E-03	-9.003E-03	2.764E-02	1.190E-02
		0.145	0.240	1	8	2.963E+00	1.688E-02	-1.128E+00	2.521E-02
		0.054	0.054	2	2	3.561E-01	-2.942E-03	6.636E-01	-1.550E-02
		0.054	0.572	2	3	-1.002E+00	1.484E-02	-5.631E-01	6.238E-02
		0.054	0.696	2	4	2.641E+00	-7.122E-03	2.176E+00	-8.926E-02
		0.054	6.214	2	5	-1.907E-01	1.189E-02	-1.817E-01	3.266E-03
		0.054	15.324	2	6	-3.039E-01	-5.330E-03	-5.328E-01	-1.674E-02
		0.054	0.166	2	7	-6.972E-02	-2.915E-03	-1.051E-01	-4.138E-03
		0.054	0.240	2	8	4.651E-01	-9.661E-03	4.883E-01	5.187E-03
		0.572	0.572	3	3	3.181E-01	-2.814E-02	9.030E-01	-8.350E-02
		0.572	0.696	3	4	-3.887E+00	7.511E-02	-1.531E+00	1.779E-01
		0.572	6.214	3	5	1.485E-01	1.306E-02	5.976E-01	2.938E-02
		0.572	15.324	3	6	-2.683E-02	4.115E-03	-9.939E-01	4.937E-03
		0.572	0.166	3	7	9.212E-02	1.760E-03	-2.146E-01	-2.856E-03
		0.572	0.240	3	8	-3.329E+00	3.318E-02	3.029E-01	6.620E-02
		0.696	0.696	4	4	-2.105E+00	-1.084E-02	-2.485E+00	8.178E-02
		0.696	6.214	4	5	-8.610E-01	2.612E-02	-3.049E+00	3.662E-02
		0.696	15.324	4	6	-1.210E+00	-1.370E-02	4.540E-01	1.082E-03
		0.696	0.166	4	7	-2.906E-01	-6.275E-03	1.694E-01	-2.562E-02
		0.696	0.240	4	8	1.024E+01	-5.115E-02	2.169E+00	-4.079E-01
		6.214	6.214	5	5	-6.127E-01	-8.809E-03	-4.744E+00	1.024E-01
		6.214	15.324	5	6	2.208E-01	-1.626E-02	2.181E+00	-2.218E-02
		6.214	0.166	5	7	-8.740E-02	1.058E-02	3.502E-01	5.062E-03
		6.214	0.240	5	8	-1.435E+00	1.076E-01	-2.728E+00	2.791E-02
		15.324	15.324	6	6	-2.849E-01	1.923E-02	-8.247E-01	6.041E-02
		15.324	0.166	6	7	1.505E-01	1.109E-03	7.886E-02	8.672E-05
		15.324	0.240	6	8	-1.482E+00	-1.513E-02	1.126E+00	-1.841E-03
		0.166	0.166	7	7	-1.049E-01	3.549E-03	-9.397E-02	-1.270E-03
		0.166	0.240	7	8	-7.195E-01	1.813E-03	1.917E-01	-8.915E-03
		0.240	0.240	8	8	2.277E+00	-5.383E-02	-3.512E+00	-1.289E-02
		Non-dimensional Results:				3.036E+00	5.691E-02	5.088E+00	1.985E-01
		Dimensional Results:				125.79 [m/s]	0.240 [s]	1.204 [Hz]	0.839 [s]

The dimensional result for the bending moment is for unit impulse. The dimensional bending moment for an impulse of 500 kN-s is therefore 62,895 kN-m.

APPENDIX C – Frigate Example

The following example is for the 124.5 m frigate studied by McTaggart *et al*. (1997).

				B.M. [N.D.]	Δt [N.D.]	f_2 [N.D.]	Tavg [N.D.]
		Constant:		1.471E+01	6.847E-02	6.433E+00	-2.088E-01
	x_i	x_j	**i**	**j**	**k=1**	**k=2**	**k=3**	**k=4**

x_i	x_j	i	j	k=1	k=2	k=3	k=4
0.119		1		-6.493E+00	2.463E-02	-3.515E+00	1.384E-01
0.040		2		-3.078E+00	9.214E-03	-4.400E+00	9.149E-02
0.496		3		5.601E+00	-3.738E-02	-2.495E+00	-2.568E-02
0.639		4		-3.784E+00	-2.388E-02	3.637E+00	7.675E-02
1.991		5		1.003E+00	-4.932E-02	4.204E+00	-8.185E-02
5.074		6		1.743E+00	-4.041E-03	7.792E-01	-5.437E-02
0.076		7		6.342E-01	-4.910E-03	1.068E-01	6.897E-03
0.228		8		-1.495E+01	7.246E-02	3.047E+00	4.325E-01
0.119	0.119	1	1	7.775E-01	-3.558E-03	8.130E-01	-3.627E-02
0.119	0.040	1	2	5.214E-01	7.021E-03	8.690E-01	8.049E-03
0.119	0.496	1	3	7.572E-01	-1.511E-02	1.817E+00	-5.415E-02
0.119	0.639	1	4	-2.657E-02	3.466E-02	-1.465E+00	1.007E-01
0.119	1.991	1	5	-1.287E-02	2.259E-04	-9.011E-01	4.703E-03
0.119	5.074	1	6	-2.201E-01	-4.417E-03	-2.498E-02	-9.429E-03
0.119	0.076	1	7	3.452E-03	-3.387E-03	1.040E-02	4.477E-03
0.119	0.228	1	8	2.304E+00	1.312E-02	-8.772E-01	1.960E-02
0.040	0.040	2	2	1.926E-01	-1.591E-03	3.588E-01	-8.384E-03
0.040	0.496	2	3	-6.391E-01	9.461E-03	-3.590E-01	3.978E-02
0.040	0.639	2	4	1.783E+00	-4.809E-03	1.469E+00	-6.026E-02
0.040	1.991	2	5	-4.494E-02	2.802E-03	-4.280E-02	7.695E-04
0.040	5.074	2	6	-7.399E-02	-1.298E-03	-1.297E-01	-4.076E-03
0.040	0.076	2	7	-2.355E-02	-9.848E-04	-3.550E-02	-1.398E-03
0.040	0.228	2	8	3.247E-01	-6.745E-03	3.409E-01	3.622E-03
0.496	0.496	3	3	2.392E-01	-2.116E-02	6.790E-01	-6.278E-02
0.496	0.639	3	4	-3.094E+00	5.980E-02	-1.219E+00	1.416E-01
0.496	1.991	3	5	4.124E-02	3.627E-03	1.660E-01	8.164E-03
0.496	5.074	3	6	-7.703E-03	1.181E-03	-2.854E-01	1.418E-03
0.496	0.076	3	7	3.669E-02	7.011E-04	-8.550E-02	-1.138E-03
0.496	0.228	3	8	-2.741E+00	2.731E-02	2.493E-01	5.450E-02
0.639	0.639	4	4	-1.774E+00	-9.134E-03	-2.095E+00	6.893E-02
0.639	1.991	4	5	-2.533E-01	7.684E-03	-8.970E-01	1.077E-02
0.639	5.074	4	6	-3.678E-01	-4.164E-03	1.380E-01	3.290E-04
0.639	0.076	4	7	-1.226E-01	-2.647E-03	7.144E-02	-1.081E-02
0.639	0.228	4	8	8.927E+00	-4.459E-02	1.891E+00	-3.556E-01
1.991	1.991	5	5	-6.290E-02	-9.043E-04	-4.870E-01	1.051E-02
1.991	5.074	5	6	2.343E-02	-1.725E-03	2.314E-01	-2.353E-03
1.991	0.076	5	7	-1.286E-02	1.558E-03	5.154E-02	7.451E-04
1.991	0.228	5	8	-4.364E-01	3.273E-02	-8.300E-01	8.491E-03
5.074	5.074	6	6	-3.124E-02	2.109E-03	-9.042E-02	6.623E-03
5.074	0.076	6	7	2.290E-02	1.687E-04	1.200E-02	1.319E-05
5.074	0.228	6	8	-4.660E-01	-4.756E-03	3.539E-01	-5.787E-04
0.076	0.076	7	7	-2.214E-02	7.489E-04	-1.983E-02	-2.679E-04
0.076	0.228	7	8	-3.138E-01	7.910E-04	8.362E-02	-3.889E-03
0.228	0.228	8	8	2.053E+00	-4.852E-02	-3.166E+00	-1.162E-02
		Non-dimensional Results:		**2.643E+00**	**8.145E-02**	**4.393E+00**	**2.461E-01**
		Dimensional Results:		**92.37**	**0.290**	**1.233**	**0.877**
				[m/s]	[s]	[Hz]	[s]

Variable definitions:

		x_i
x1	B/L	0.119
x2	T/L	0.040
x3	C_B	0.496
x4	C_{WP}	0.639
x5	γ_4	1.991
x6	$I/[0.01\ L]^4$	5.074
x7	$A_{SHEAR}/[0.01\ L]^2$	0.076
x8	k_{yy}/L	0.228

The dimensional result for the bending moment is for unit impulse. The dimensional bending moment for an impulse of 500 kN-s is therefore 46,183 kN-m.